Noble-metal-free photocatalysts MoS_2-graphene/CdS mixed nanoparticles/nanorods morphology with high visible light efficiency for H_2 evolution

Miaomiao Liu, Fengyan Li,* Zhixia Sun, Lifang Ma, Lin Xu,* and Yuanhong Wang

Key Laboratory of Polyoxometalate Science of Ministry of Education, Department of Chemistry, Northeast Normal University, Changchun, Jilin 130024, P. R. China. Fax: +86-431-85099765; Tel: +86-431-85098760; E-mail: lify525@nenu.edu.cn; linxu@nenu.edu.cn

Experimental details

Synthesis of MoS_2 photocatalyst. Layered MoS_2 were prepared by a routine hydrothermal method. All the reagents were of analytical grade and used without further purification. In a typical synthesis of MoS_2, 1 mmol of $Na_2MoO_4 \cdot 2H_2O$ and 5 mmol of thiourea were dissolved in 50 mL of distilled water and 10ml ethanol, the solution was transferred into a 100 mL Teflon-lined autoclave and held at 210 ºC for 24 h. The black precipitate was collected by filtrated and washed with deionized water for three times, followed by drying 12h at 80 ºC.

Synthesis of MoS_2-graphene/CdS nanoparticles and nanorods (M-G/CdS(NP-NR)) photocatalyst. The composite samples were also synthesized by a hydrothermal method. CdS was synthesized according to the literature method[1] except being kept at 60 ºC for 12 h after separation. Graphene oxide (GO) was synthesized from natural graphite powder (>99.8%, Alfa Aesar) by a modified Hummers' method.[2] In a typical synthesis of M-G/CdS(NP-NR) photocatalyst, 0.2g of CdS, 0.0095g MoS_2 and 0.0005g GO were dispersed in 30 mL of deionized water and 10 ml ethanol. After ultrasonication for 1 h, the mixture was transferred into a 50 mL Teflon-lined autoclave followed by hydrothermal treatment at 180 ºC for 12h. The dark green solids were collected by filtrated and washed with deionized water for several times, followed by drying overnight at 80 ºC. Similarly, a series of the M-G/CdS (NP-NR) composites was prepared by changing the ratio of MoS_2 and graphene in co-catalyst under the same conditions but replacing 95M-5.0G with (100-x)M-xG or GO. Moreover, in order to further investigate the effect of the content of the MoS_2-graphene (95M-5.0G) co-catalyst on the photocatalytic hydrogen activity of CdS, the mass ratio of 95M-5.0G/CdS was changed from 0% to 10.0% (0, 1.0, 5.0 and 10.0 wt%) by varying the amount of 95M-5.0G.

Synthesis of MoS_2-graphene/CdS nanoparticles (M-G/CdS(NP)) photocatalyst. The M-G/CdS(NP) sample was synthesized similar to the synthesis of M-G/CdS(NP-NR) except the hydrothermal treatment at 160 ºC for 12h.

Synthesis of MoS_2-graphene/CdS nanorods (M-G/CdS(NR)) photocatalyst. CdS nanorods were prepared according to the literature.[3] The M-G/CdS(NR) sample was synthesized similar to the synthesis of M-G/CdS(NP-NR) except using CdS nanorods instead of CdS nanoparticles as the starting materials.

Photocatalytic reaction. In a typical photocatalytic experiment, 0.1 g photocatalyst was well suspended with constant stirring in a 160 mL of aqueous solution containing 20 vol% of lactic acid (85-90% aqueous solution, Alfa Aesar). Prior to irradiation, the suspension of the catalyst was bubbled with nitrogen through the reactor for 30 min to completely remove the dissolved oxygen and to assure anaerobic conditions. After thoroughly degassed, the suspension was irradiated by a 300 W Xe lamp (PLS-SXE300, Beijing Trusttech Co. Ltd.) which is equipped with an optical filter (UV-CUT 400 nm) to cut off the light in the ultraviolet region. The temperature of the reaction solution was maintained at 20 ºC by a flow of cooling water. The irradiation power after the cutoff filter (λ > 400 nm) and the band-pass filter (420 nm) were measured to be 63 and 1.9 mW cm^{-2}, respectively. The apparent quantum yield (QY) was measured under the same reaction conditions except a band-pass interference filter (420 nm). The following equation was used to calculate the QY.

$$\text{QY }(\%) = \frac{\text{The number of evolved hydrogen molecules} \times 2}{\text{The number of incident photons}} \times 100$$

Characterization

Powder X-ray diffraction (XRD) measurements were recorded ranging from 5 to 80° at room temperature on a Siemens D5005 diffractometer with Cu-Kα (λ = 1.5418 Å) radiation. The X-ray photoelectron spectra (XPS) were recorded on a USWHA150 photoelectron spectroscope using monochromatic Al Kα (1486.6 eV) radiation. The ultraviolet-visible diffuse reflectance spectra were obtained using a CARY 500 scan UV-vis-NIR spectrophotometer. Morphology and composition analyses were carried out on a FEI quanta 250 field emission scanning electron microscopy (SEM). Transmission electron microscopy (TEM) images were obtained on a JEM-2100F microscope with an accelerating voltage of 200 kV. Elemental analyses (C, H and N) were performed on Flash EA 112 CHN Elemental Analyzer and metal elemental analyses were determined by a Leaman inductively coupled plasma (ICP) spectrometer. The hydrogen evolved was analyzed with a gas chromatograph (Agilent 6890GC, thermal conductivity detector, Ar carrier). Photocurrents were measured using a CHI660C electrochemical analyzer with a standard three-electrode system using the prepared samples as the working electrodes with an active area of ca. 1.0 cm^2, a Pt foil as the counter electrode, and Ag/AgCl (saturated KCl) as a reference electrode and 0.1 M Na_2SO_4 electrolyte. The working electrodes were prepared as follows: 0.05 g of the sample and 1 ml dimethyl formamide (DMF) were mixed after ultrasonication for 30 min. Then, the mixture was coated onto a 1 cm×1 cm Indium Tin Oxides (ITO) glass electrode by the spin-coating technique. At last, these electrodes were dried in the air and calcined at 200 ºC for 2h. The BET surface area was determined using adsorption data in the relative pressure (P/P_0) range of 0.05-0.3. The desorption data were used to determine the pore size distribution *via* the Barret-Joyner-Halender (BJH) method. [4] The nitrogen adsorption volume at the relative pressure (P/P_0) of 0.99 was used to determine the single-point pore volume and the average pore size.

References:

[1] H. J. Yan, J. H. Yang, G. J. Ma, G. P. Wu, X. Zong, Z. B. Lei, J. Y. Shi, C. Li, *J. Catal.*, 2009, **266**, 165.

[2] L. J. Cote, F. Kim, J. X. Huang, *J. Am. Chem. Soc.*, 2009, **131**, 1043–1049.

[3] S. Rohit, P. Bonamali, *Mater. Res. Bull.*, 2013, **48**, 1403-1410.

[4] K. S. W. Sing , D. H. Everett, R. A. W. Haul, L. Moscou, T. Siemieniewska, *Pure Appl. Chem.*, 1985, **57**, 603-619.

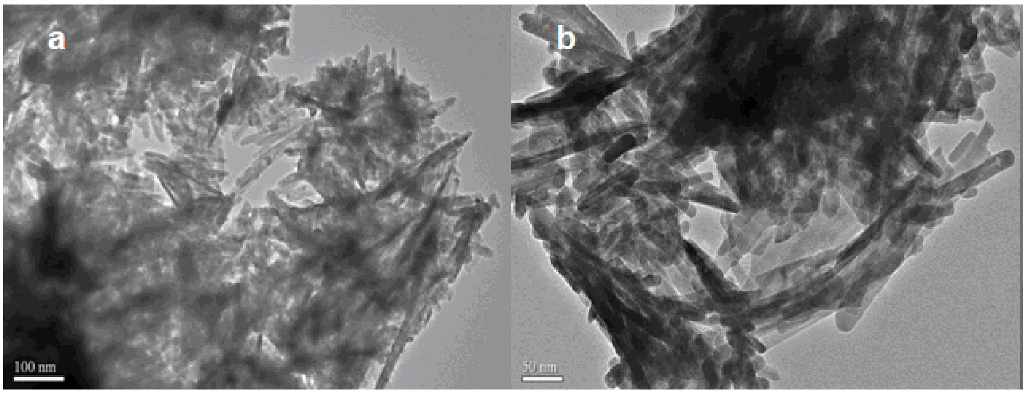

Fig. S1 TEM images of M-G/CdS(NR).

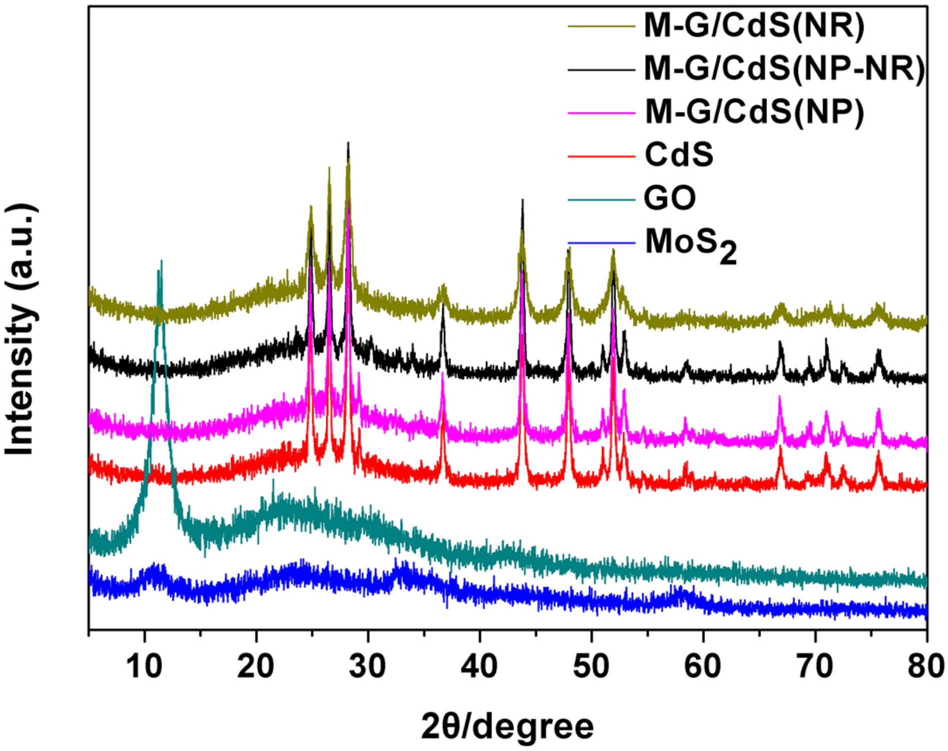

Fig. S2 The XRD patterns of GO, MoS$_2$, CdS, M-G/CdS(NP), M-G/CdS(NR) and M-G/CdS(NP-NR).

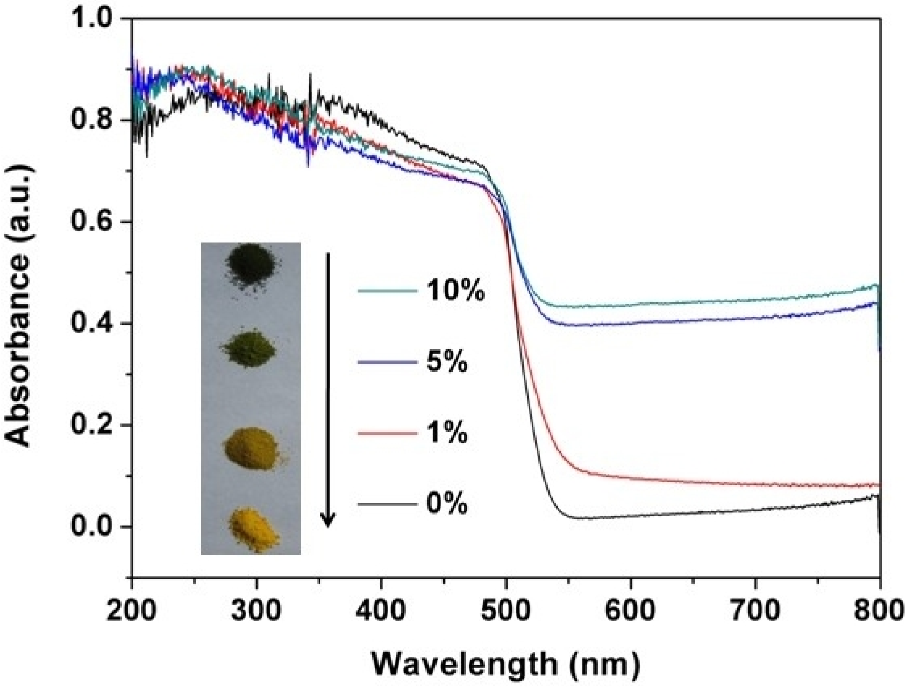

Fig. S3 UV-vis diffuse reflection spectra of M-G/CdS(NP-NR) composite photocatalysts with different amount of M-G hybrid (M:G=95:5.0), 0%, 1%, 5%, 10%.

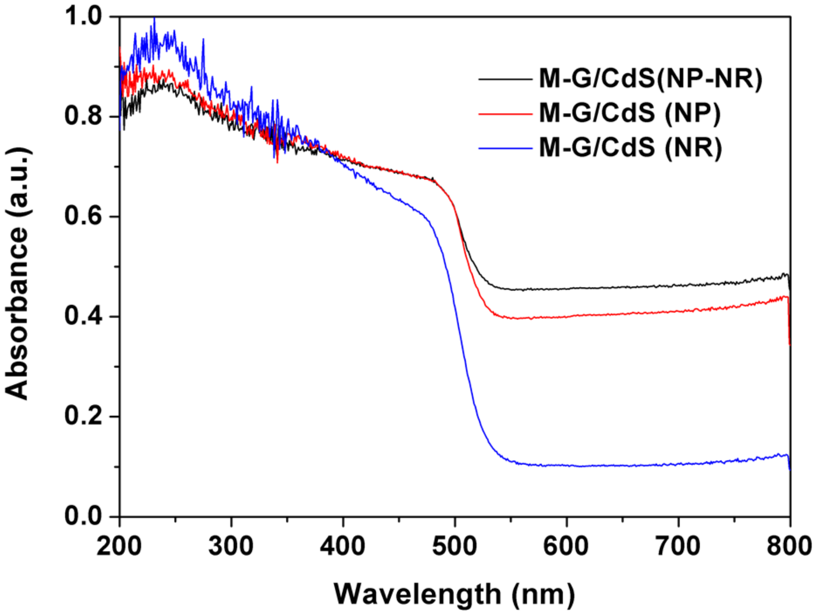

Fig. S4 UV-vis diffuse reflection spectra of M-G/CdS(NP), M-G/CdS(NR), and M-G/CdS(NP-NR) composite photocatalysts.

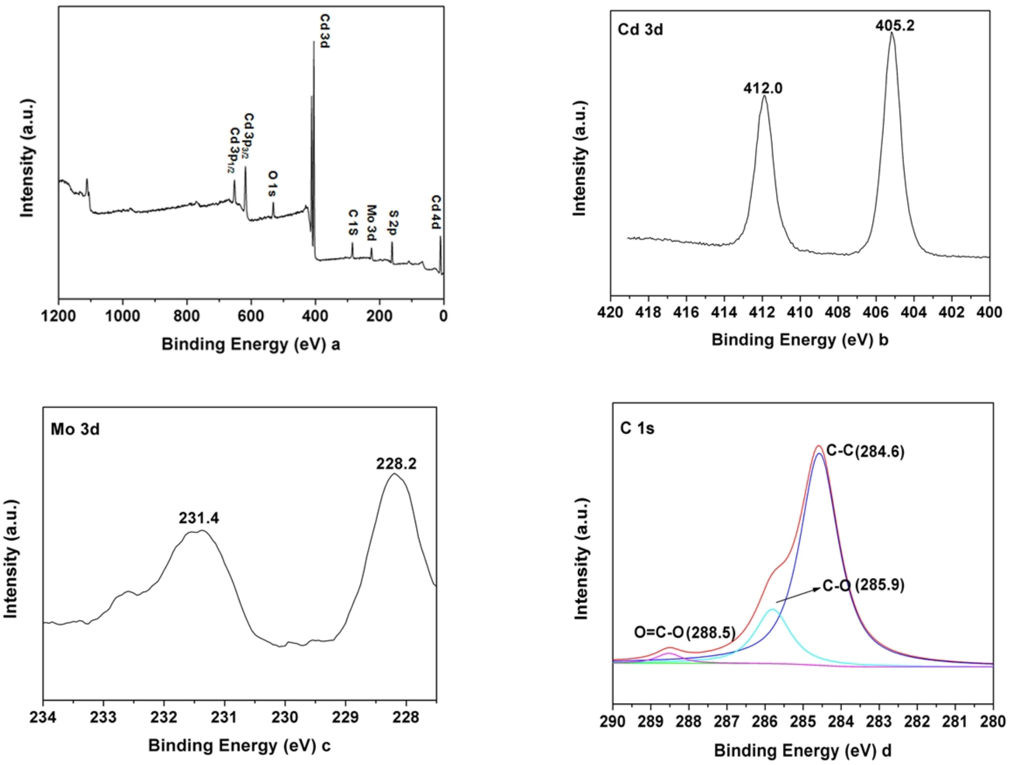

Fig. S5 (a) XPS survey spectrum of M-G/CdS(NP-NR). (b) The high-resolution XPS spectra of Cd 3d, (c) The high-resolution XPS spectra of Mo 3d, and (d) C 1s in M-G/CdS(NP-NR).

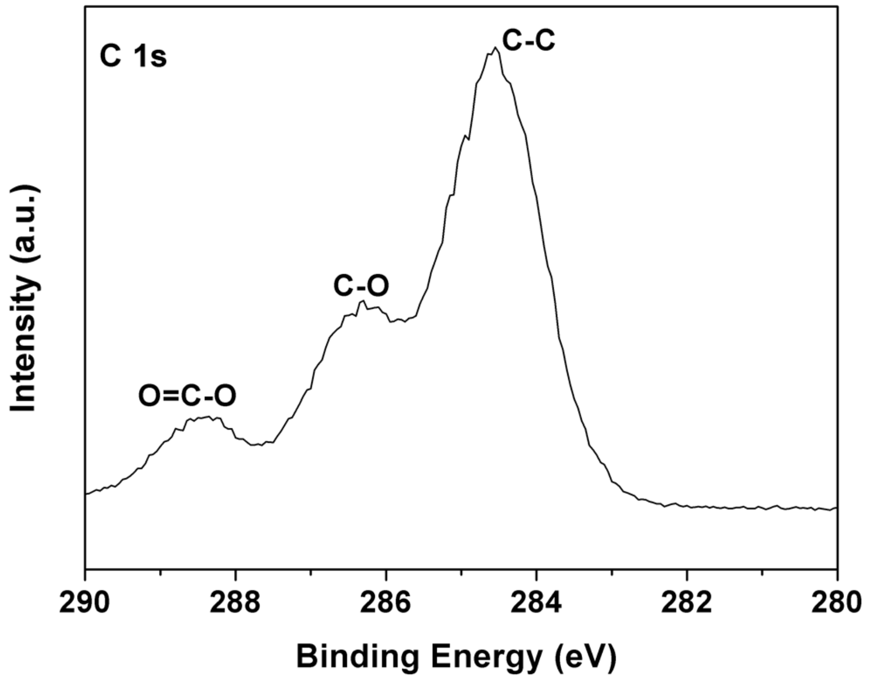

Fig. S6 The C1s XPS spectrum of the graphene oxide.

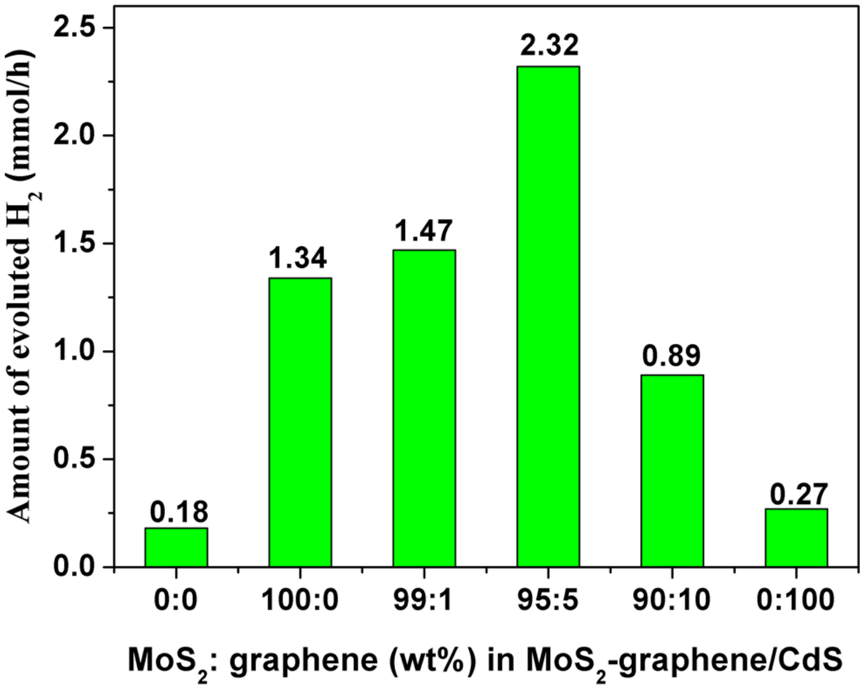

Fig. S7 Photocatalytic H_2 evolution of composites M-G/CdS(NP-NR). Photocatalytic H_2 production experiments were performed in 20 vol% lactic acid solutions under visible light using the photocatalyst M-G/CdS(NP-NR) composites with different MoS_2 and graphene contents as co-catalyst.

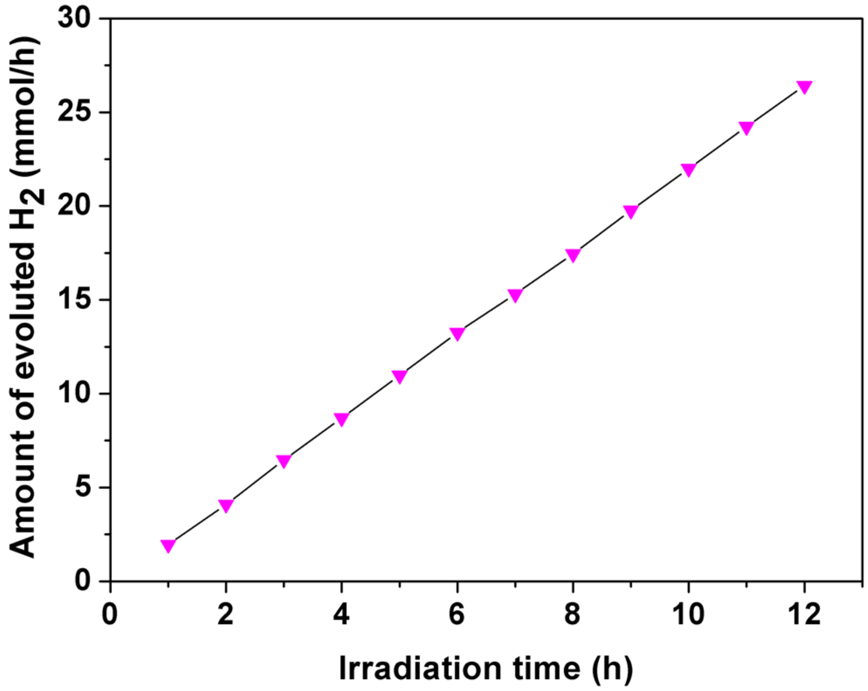

Fig. S8 The amount of H_2 evolved on M-G/CdS(NP-NR) in 12 h of continuous reaction.

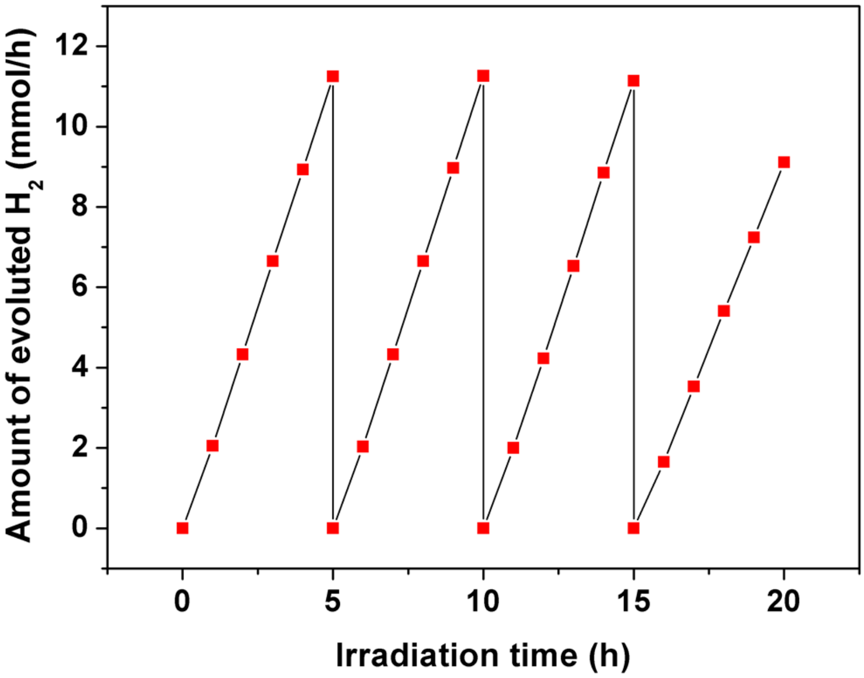

Fig. S9 Long-time stability test of M-G/CdS(NP-NR) for hydrogen evolution. Reaction condition: 0.1 g catalyst; 160 ml 20 vol% lactic acid aqueous solution; light source: 300 W Xe lamp (λ > 400 nm). The reaction solution was replaced by a new one after 5 h of the reaction.

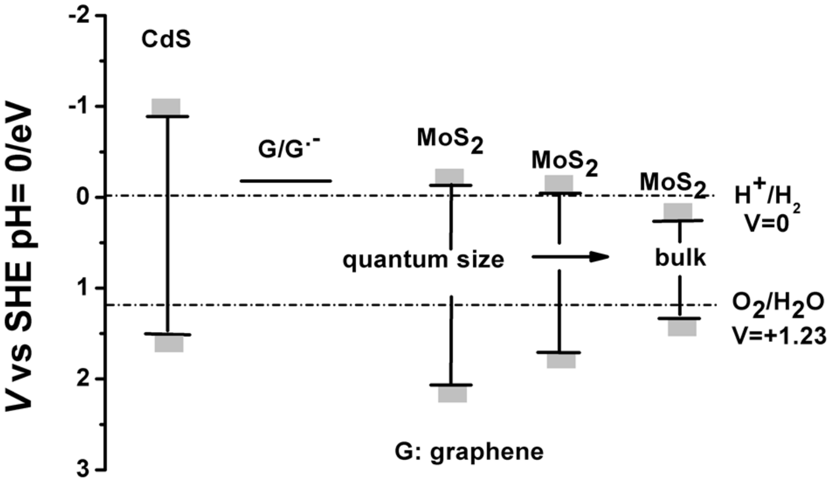

Fig. S10 Schematic illustration of the potential and band positions in the composite photocatalyst M-G/CdS(NP-NR).

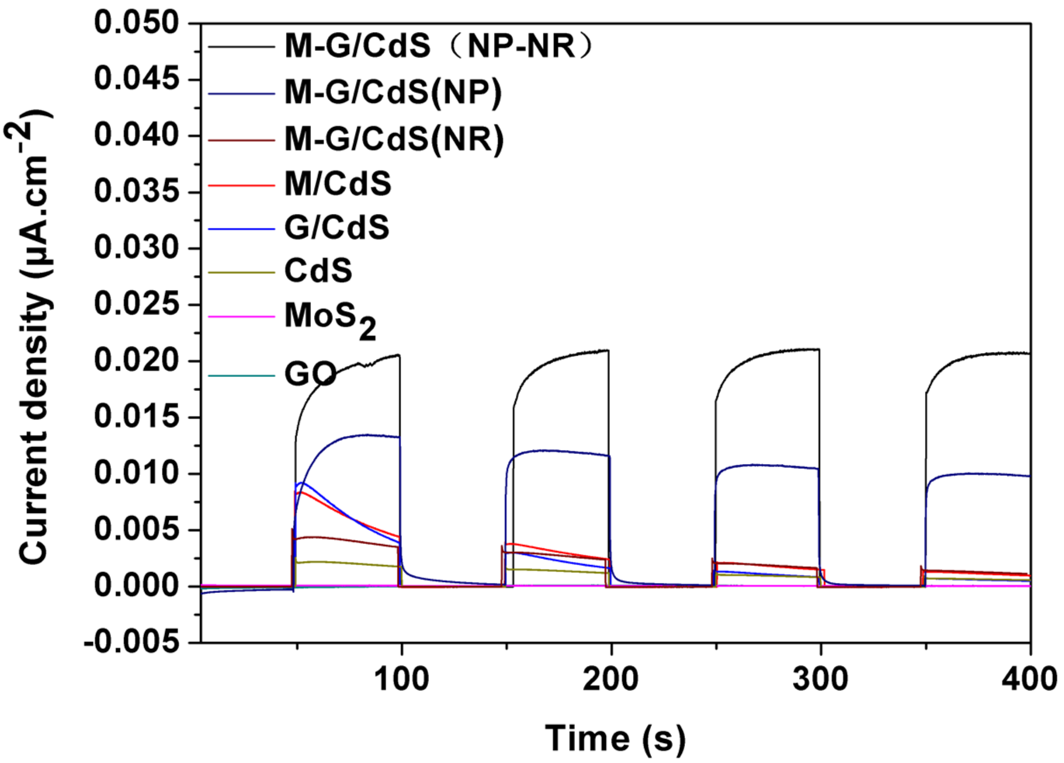

Fig. S11 Transient photocurrent responses of the films of M-G/CdS(NP-NR), M-G/CdS(NR), M-G/CdS(NP), M/CdS, G/CdS, GO, MoS_2 and CdS. A three-electrode system was employed in a quartz cell with a Ag/AgCl (saturated KCl) electrode as the reference electrode, a platinum foil as the counter electrode, the film assembled ITO glass as the working electrode and 0.1 M Na_2SO_4 electrolyte; light source: 300 W Xe lamp ($\lambda > 400$ nm).

The photocurrent response appears for the samples under visible light illumination without any bias potential. This indicates that most of the photogenerated electrons are transported to the working electrode surface across the sample to produce photocurrent under irradiation. For the pure CdS sample, the photocurrent curve has an obvious photocurrent spike at the initial time of irradiation. Subsequently, a continuous decrease in the photocurrent with time can be observed, which indicates that the recombination process occurs. As a result, the pure CdS sample exhibits relative weak photocurrent because of the high recombination rate of electrons and holes. The introduction of MoS_2 or graphene can improve the photocurrent response of the samples (M/CdS and G/CdS), however, obvious photocurrent decay can still be observed. As for the M-G/CdS(NP) sample, the photocurrent is increased further and exhibits a slight decay, indicating the improved charge transfer from CdS to graphene and/or MoS_2, and then to the working electrode surface. The M-G/CdS(NP-NR) sample shows the highest photocurrent density. It suggests that MoS_2 and graphene, together with CdS NP/NR, can effectively separate the photogenerated electrons and holes, consequently reducing the recombination rate of photo-excited carriers and enhancing the production of photocurrent. Therefore, it is not surprising that the M-G/CdS(NP-NR) sample exhibits the highest photocatalytic H_2 evolution rate.

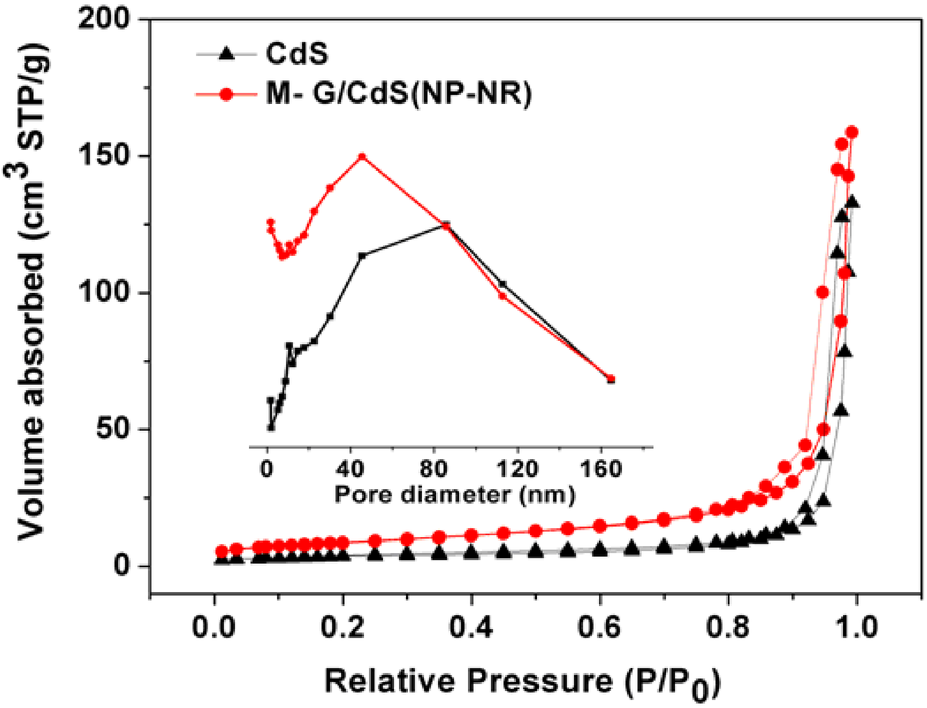

Fig. S12 Nitrogen adsorption-desorption isotherms and the corresponding pore-size distribution curves (inset) of samples CdS and M-G/CdS(NP-NR).

The pore structure and BET surface of the pure CdS, M-G/CdS(NP) and M-G/CdS(NP-NR) were investigated using nitrogen sorption measurements. After loading 5 wt % M-G, the BET surface areas of both M-G/CdS(NP) and M-G/CdS(NP-NR) increased, which is in accordance with the improved dispersion observed from the SEM images. Moreover, the BET surface area of M-G/CdS(NP-NR) is higher than that of M-G/CdS(NP) owing to the existence of 1D CdS NRs. The nitrogen adsorption-desorption isotherms for M-G/CdS(NP-NR) displays narrow hysteresis loops at relative pressures close to unity, indicating the presence of large mesopores and macropores, which can be categorized as type IV according to IUPAC classification. The pore size distribution curve of M-G/CdS(NP-NR) exhibits a wide pore size distribution from 2-160 nm in the mesoporous and macroporous region, which will provide efficient transport pathways for reactant and product molecules. The shape of the hysteresis loop is of a type H_3, associated with the presence of slit-like pores due to aggregation of CdS NPs and NRs. The BET specific surface areas, pore volumes, and average proe size of all the samples are summarized in Table S1.

Table S1 Effects of MoS_2 and graphene in the M-G/CdS(NP), M-G/CdS(NR), M-G/CdS(NP-NR) on the physiochemical properties and H_2-production rate of the composites.

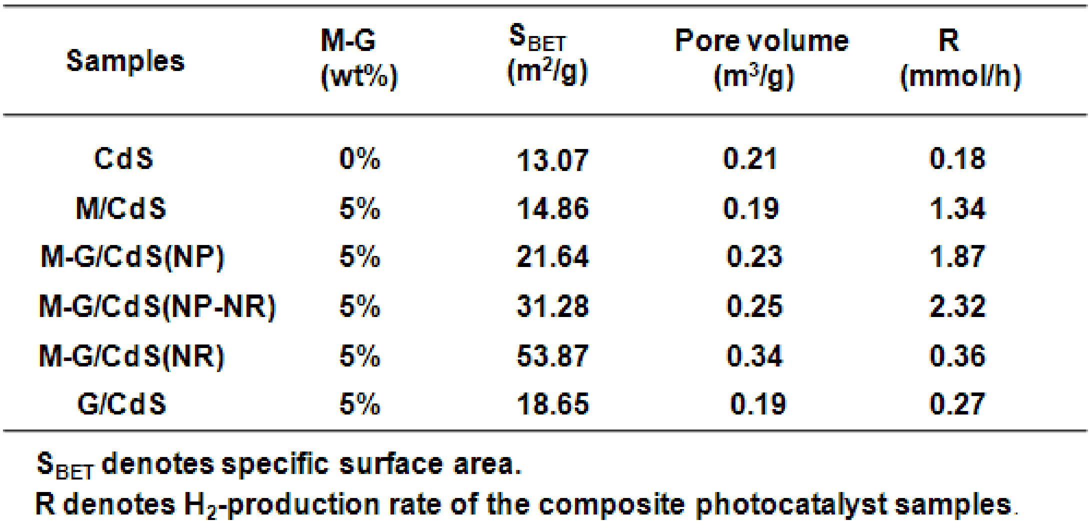

Samples	M-G (wt%)	S_{BET} (m^2/g)	Pore volume (m^3/g)	R (mmol/h)
CdS	0%	13.07	0.21	0.18
M/CdS	5%	14.86	0.19	1.34
M-G/CdS(NP)	5%	21.64	0.23	1.87
M-G/CdS(NP-NR)	5%	31.28	0.25	2.32
M-G/CdS(NR)	5%	53.87	0.34	0.36
G/CdS	5%	18.65	0.19	0.27

S_{BET} denotes specific surface area.
R denotes H_2-production rate of the composite photocatalyst samples.

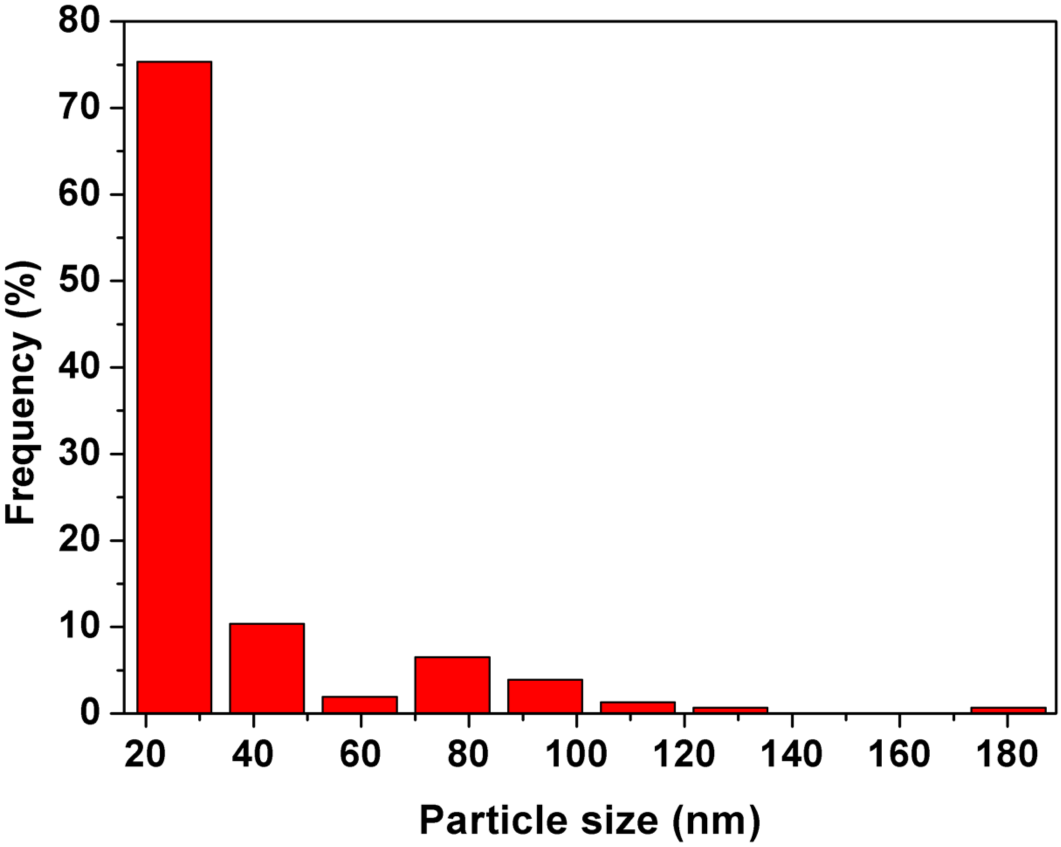

Fig. S13 Particle size distribution of CdS crystallites obtained by image analysis of SEM micrographs. The size distributions of the M-G/CdS(NP-NR) samples are calculated by counting at least 150 particles/rods from the SEM images. The amount of CdS nanorods (the length > 80 nm) is about 6% of the nanoparticles/nanorods mixture.